Nanoscale

PAPER

View Article Online
View Journal | View Issue

Cite this: *Nanoscale*, 2024, **16**, 9361

Construction of novel Ag(0)-containing silver nanoclusters by regulating auxiliary phosphine ligands†

Qing-Qing Ma,[a] Xue-Jing Zhai,[a] Jia-Hong Huang,[a] Yubing Si,[a] Xi-Yan Dong,*[a,b] Shuang-Quan Zang*[a] and Thomas C. W. Mak[a,c]

Received 17th March 2024,
Accepted 11th April 2024

DOI: 10.1039/d4nr01152j

rsc.li/nanoscale

Controlled synthesis of metal clusters through minor changes in surface ligands holds significant interest because the corresponding entities serve as ideal models for investigating the ligand environment's stereochemical and electronic contributions that impact the corresponding structures and properties of metal clusters. In this work, we obtained two Ag(0)-containing nanoclusters (**Ag_{17}** and **Ag_{32}**) with near-infrared emissions by regulating phosphine auxiliary ligands. **Ag_{17}** and **Ag_{32}** bear similar shells wherein **Ag_{17}** features a trigonal bipyramid Ag_5 kernel while **Ag_{32}** has a bi-icosahedral interpenetrating an Ag_{20} kernel. **Ag_{17}** and **Ag_{32}** showed a near-infrared emission (NIR) of around 830 nm. Benefiting from the rigid structure, **Ag_{17}** displayed a more intense near-infrared emission than **Ag_{32}**. This work provides new insight into the construction of novel superatomic silver nanoclusters by regulating phosphine ligands.

Introduction

Metal nanoclusters have attracted wide attention because of their atom-precise structures and quantum size effects, which provide an ideal platform for investigating the connection between simple metal complexes and bulk metal nanoparticles.[1–16] In addition, their potential applications in optics,[17–20] catalysis,[21–25] and biomedicine[26–28] encourage us to synthesize novel structured nanoclusters to exploit versatile properties. Among these, nanoclusters with valence electron structures similar to atomic electron structures are considered "superatomic nanoclusters".[29–34] The regulation of superatomic nanocluster structures and nuclearities is beneficial for broadening the diversity of properties and facilitating the exploration of the structure–property correlation at the atomic level. The synthesis of structurally well-defined Ag(0)-containing nanoclusters has been performed for over a decade, but the instability of silver nanoclusters restricts their structural modulation.[35–39]

Currently, several effective methods have been developed to fine-tune the nanocluster structures, including heterometal doping,[40–42] ligand engineering,[43–48] counter ion template,[49–52] and so on. The ligand engineering strategy is considered one of the most effective ways to regulate the structure and supramolecular assembly of nanoclusters. Ligand engineering strategies have been reported to adjust the structures and properties of nanoclusters by the steric hindrance effect, electron-withdrawing and donating effects, *etc.*[53,54] Surface ligand regulation includes the primary ligands (such as thiolate ligands) and auxiliary ligands. Although manipulating primary ligands is effective for achieving higher nuclearities and electron counts, it is often a time-consuming and laborious process.[55–57] In contrast, the use of readily available auxiliary ligands, such as phosphine ligands, has the potential to be more efficient.[58,59]

Herein, by regulating the auxiliary phosphine ligands, we synthesized two cases of superatomic silver nanoclusters, formulated as $[Ag_{17}(L)_{12}(PPh_3)_6](NO_3)_3$ (L = quinoline-2-thiol (deprotonation)-4-carboxyl, PPh_3 = triphenylphosphine, denoted as **Ag_{17}**) and $[Ag_{32}(L)_{18}(P(Ph\text{-}^{p}CH_3)_3)_6Cl_2](NO_3)_4$ (L = quinoline-2-thiol (deprotonation)-4-carboxyl, $P(Ph\text{-}^{p}CH_3)_3$ = tri-*p*-tolylphosphine, denoted as **Ag_{32}**). The atomically precise structures of two silver nanoclusters were determined by single-crystal X-ray diffraction (SC-XRD) and further confirmed by electrospray ionization mass spectrometry (ESI-MS) measurements. Both **Ag_{17}** and **Ag_{32}** feature $Ag_4L_4P_2$ unit-based surface structures, but **Ag_{17}** has an Ag_5 trigonal bipyramid kernel while **Ag_{32}** has the Ag_{20} inner core with the fusion of

[a]College of Chemistry, Zhengzhou University, Zhengzhou 450001, China. E-mail: zangsqzg@zzu.edu.cn, dongxiyan0720@hpu.edu.cn
[b]College of Chemistry and Chemical Engineering, Henan Polytechnic University, Jiaozuo 454000, China
[c]Department of Chemistry, The Chinese University of Hong Kong, Shatin, New Territories, Hong Kong, SAR, China

†Electronic supplementary information (ESI) available: Fig. S1–S20 and Tables S1–S4 for experimental details, detailed crystallographic structures, PXRD, and UV-vis spectra. CCDC 2327808 and 2327952. For ESI and crystallographic data in CIF or other electronic format see DOI: https://doi.org/10.1039/d4nr01152j

two classical Ag_{13} icosahedrons. Both of them have emissions in the near-infrared region under ambient temperature. The quantum yield of the **Ag_{17}** solution is 3.09%, while the quantum yield of the **Ag_{32}** solution is below 0.1%. **Ag_{17}** shows superior luminescence properties compared to **Ag_{32}** due to its rigid surface structure.

Experimental section

Materials and reagents

All chemicals and solvents obtained from suppliers were used without further purification. All solvents were analytical-grade reagents. Silver nitrate ($AgNO_3$, 98%), triphenylphosphine (PPh_3, 97%), tri-*p*-tolylphosphine ($P(Ph\text{-}^pCH_3)_3$, 97%), 2-chloroquinoline-4-carboxylic acid (2-Cl-4-COOH-QL, 96%), thiourea (CH_4N_2S, 99%), sodium borohydride ($NaBH_4$, 98%), sodium hydroxide (NaOH, 98%), and hydrochloric acid (HCl, 38%) were used.

Synthesis of quinoline-2-thiol (deprotonation)-4-carboxyl (L)

L was synthesized according to the procedures described in the literature.[60] 2-Cl-4-COOH-QL (1 mol) was added to the EtOH solution of thiourea (1.2 mol) and the mixture was refluxed for 15–30 min. Then the solution was diluted to twice its volume with H_2O, and the yellow product obtained was dissolved in 10% NaOH. The yellow filtrate was acidified with 10% HCl and the yellow precipitate obtained was collected by filtration, washed with H_2O, and dried. It was recrystallized from EtOH to give yellowish-orange needles. The ^1H NMR spectra confirmed the structure (Fig. S1, ESI†). δ = 13.99 (s, 1H), 8.34–8.33 (d, 1H), 7.69–7.68 (d, 2H), 7.58 (d, 1H), 7.43–7.40 (m, 1H).

Synthesis of $[Ag_{17}(L)_{12}(PPh_3)_6](NO_3)_3$ (Ag_{17})

$AgNO_3$ (12 mg, 0.07 mmol) was dissolved in a mixed solvent of 4 mL of methanol and 4 mL of dichloromethane at room temperature. Then L (10 mg, 0.05 mmol) and PPh_3 (13 mg, 0.05 mmol) were added under vigorous stirring to afford Ag–S–P complex. About 5 min later, freshly prepared $NaBH_4$ (2 mg, 0.052 mmol) in 1 mL of methanol was added dropwise under stirring. The color of the solution changed from yellow to brown–black. Five hours later, the brown–black solution was collected after centrifuging. The mixture evaporated slowly at room temperature and orange crystals were obtained for five days. Yield: 15% (based on Ag). Elemental analysis (found (calcd.), %; based on $C_{228}H_{162}Ag_{17}N_{15}O_{33}P_6S_{12}$): C, 44.86 (45.31); H, 2.62 (2.70); N, 3.19 (3.48); S, 6.48 (6.37); O 8.54 (8.74).

Synthesis of $[Ag_{32}(L)_{18}(P(Ph\text{-}^pCH_3)_3)_6Cl_2](NO_3)_4$ (Ag_{32})

$AgNO_3$ (17 mg, 0.1 mmol) was dissolved in a mixed solvent of 4 mL of methanol and 4 mL of dichloromethane at room temperature. Then L (12 mg, 0.06 mmol) and $P(Ph\text{-}^pCH_3)_3$ (25 mg, 0.082 mmol) were added under vigorous stirring. About 5 min later, freshly prepared $NaBH_4$ (2 mg, 0.052 mmol) in 1 mL of methanol was added dropwise under stirring. The color of the solution changed from yellow to brown–black. Five hours later, the brown–black solution was collected after centrifuging. The mixture evaporated slowly at room temperature and black block crystals were obtained for five days. Yield: 27% (based on Ag). Elemental analysis (found (calcd.), %; based on $C_{306}H_{234}Ag_{32}N_{22}O_{48}P_6S_{18}Cl_2$): C, 39.91 (39.64); H, 2.32 (2.54); N, 3.41 (3.32); S, 6.39 (6.22); O, 8.35 (8.28).

Characterization

^1H NMR spectroscopy was carried out on a Bruker 400 spectrometer operating at 600 MHz with DMSO-d6 as the solvent. Electrospray ionization mass spectrometry (ESI-MS) was performed on a X500R QTOF spectrometer. Powder X-ray diffraction (PXRD) patterns of the samples were recorded on a D/MAX-3D diffractometer. Elemental analyses (EA) were carried out with a PerkinElmer 240 elemental analyzer. Fourier transform infrared (FT-IR) spectra were recorded on a Bruker ALPHA II spectrometer. UV-vis absorption spectra were obtained by means of a Hitachi UH4150 UV-visible spectrophotometer. The NIR luminescence spectra were measured with an Edinburgh FLS 980 fluorescence spectrometer. The luminescence lifetime was measured on an Edinburgh FLS 980 fluorescence spectrometer operating in time-correlated single-photon counting (TCSPC) mode. The quantum yield (QY) was measured using an integrating sphere on an Edinburgh FLS 980 fluorescence spectrometer. X-ray photoelectron spectroscopy (XPS) was conducted using a Thermo ESCALAB 250XI with Al Kα radiation as the excitation source. C 1s calibrated binding energies at 284.8 eV. Energy-dispersive spectroscopy and elemental mapping measurements were performed *via* a Zeiss Sigma 500.

Results and discussion

Ag_{17} and **Ag_{32}** were prepared by a one-pot reduction method. Briefly for **Ag_{17}**, $AgNO_3$ was dissolved in a mixed solvent of methanol and dichloromethane at room temperature followed by the addition of L and PPh_3 under vigorous stirring to afford the Ag–S–P complex. Subsequently, freshly prepared $NaBH_4$ in methanol was added dropwise under stirring. The color of the solution changed from yellow to brown–black. The raw product solution was collected after centrifuging. Orange crystals were obtained by evaporating slowly in darkness for five days. **Ag_{32}** was prepared by a similar method but with $P(Ph\text{-}^pCH_3)_3$ instead of PPh_3, and the black block crystals of **Ag_{32}** were obtained (Scheme 1).

The chemical compositions of **Ag_{17}** and **Ag_{32}** were confirmed by electrospray ionization mass spectroscopy (ESI-MS). As shown in Fig. 1a, the ESI-MS spectrum of **Ag_{17}** shows a prominent signal at *m*/*z* 1952.70, which corresponds to the $[Ag_{17}(PPh_3)_6(L)_{12}]^{3+}$ species (calcd. *m*/*z* 1952.69). **Ag_{17}** exhibits a 2-electron configuration (17 − 12 − 3 = 2e). As shown in Fig. 1b, the ESI-MS spectrum of **Ag_{32}** shows a prominent signal at *m*/*z* 2256.26, which corresponds to the

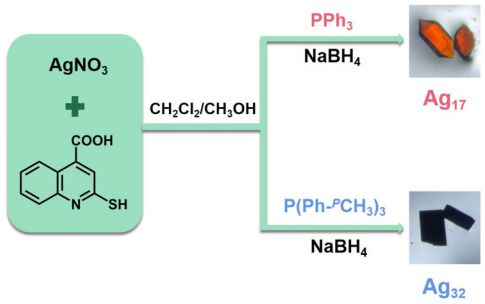

Scheme 1 Synthetic routes for Ag_{17} and Ag_{32}.

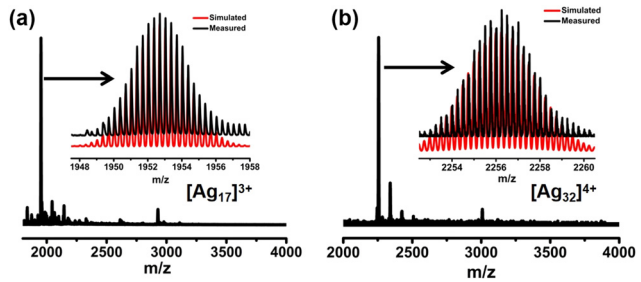

Fig. 1 (a) Positive-ion mode ESI-MS of Ag_{17} in CH_3OH. (Inset) Measured (black line) and simulated (red line) isotopic distribution patterns of the molecular ion peak. (b) Positive-ion mode ESI-MS of Ag_{32} in CH_3OH. (Inset) Measured (black line) and simulated (red line) isotopic distribution patterns of the molecular ion peak.

$[Ag_{32}(P(Ph\text{-}^{p}CH_3)_3)_6(L)_{18}Cl_2]^{4+}$ species (calcd. m/z 2256.24). It bears an eight-electron closed-shell (32 − 18 − 2 − 4 = 8e) structure. The presence of NO_3^- in Ag_{17} and Ag_{32} was also confirmed by Fourier transform infrared (FT-IR) spectra and negative-ion mode ESI-MS spectra (Fig. S2 and S3, ESI†). Powder X-ray diffraction (PXRD) further verified the phase purity of Ag_{17} and Ag_{32} (Fig. S4, ESI†). X-ray photoelectron spectroscopy (XPS) and energy dispersive X-ray spectrometry (EDS) elemental mapping of Ag_{17} and Ag_{32} revealed all of the expected elements and the presence of Ag(0) in Ag_{17} and Ag_{32} (Fig. S5–S8, ESI†).

Single-crystal X-ray diffraction (SC-XRD) analysis revealed that Ag_{17} crystallized in the $P\bar{3}1c$ space group. The overall structure of Ag_{17} shows a 3-fold rotational symmetry (Fig. 2a and Fig. S9, ESI†). Ag_{17} has an Ag_5 trigonal bipyramid (Fig. 2b) covered by the $Ag_{12}(L)_{12}(PPh_3)_6$ shell (Fig. S10a, ESI†). The 3-fold axis passes through the top and bottom of the two vertexes of the kernel. Thus, the $Ag_{12}(L)_{12}(PPh_3)_6$ shell could be regarded as a trimeric structure of the $Ag_4L_4(PPh_3)_2$ unit (Fig. 2c and d). Each $Ag_4L_4(PPh_3)_2$ is located on one side of the trigonal bipyramid. The thiolates in the "equatorial" position of the kernel adopt a μ_4 bridging mode and the other thiolates near the vertexes of the kernel adopt a μ_3 bridging mode. The Ag atoms located above the triangular Ag_3 face of the Ag_5 trigonal bipyramid are quadruply coordinated to three sulfur atoms of three L ligands and one phosphorus atom of PPh_3. The other Ag atoms located near vertexes of the kernel are quadruply coordinated to two sulfur atoms and two nitrogen atoms of the neighboring two L ligands. In addition, the free carboxylic acid functional groups impart potential for post-modification to Ag_{17}.

Ag_{32} adopts the $P\bar{4}3n$ space group with a formula $[Ag_{32}(P(Ph\text{-}^{p}CH_3)_3)_6(L)_{18}Cl_2]$. The overall structure of Ag_{32} is shown in Fig. 2e. Structurally, Ag_{32} features an Ag_{20} kernel, which is the fusion of two classical Ag_{13} icosahedrons (Fig. 2f). Alternatively, the Ag_{20} kernel could also be regarded as the fusion of the Ag_5 trigonal bipyramid by sharing the icosahedral central Ag atom. Probably due to Ag_{17} and Ag_{32} having an Ag_5 trigonal bipyramid-based kernel, they have similar surface structures (Fig. S10b, ESI†). Compared to Ag_{17} with a trimeric structure of $Ag_4L_4(PPh_3)_2$ units, Ag_{32} has three monomeric

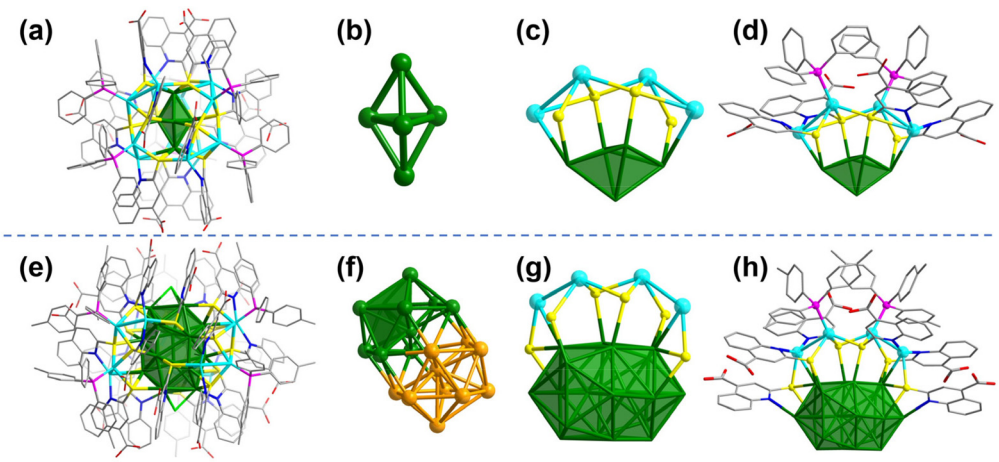

Fig. 2 (a) The overall structure of Ag_{17}. (b) The Ag_5 kernel of Ag_{17}. (c) The Ag_4S_4 motif of Ag_{17}. (d) The Ag_{17} peripheral $Ag_4L_4(PPh_3)_2$ unit. (e) The overall structure of Ag_{32}. (f) The Ag_{20} kernel of Ag_{32} (the polyhedron highlighted is an Ag_5 unit). (g) The Ag_4S_6 motif of Ag_{32}. (h) The Ag_{32} peripheral $Ag_4L_6(P(Ph\text{-}^{p}CH_3)_3)_2$ unit. Atom colors: Ag, dark green, turquoise and orange; P, purple; N, blue; S, yellow; Cl, light green; C, gray; O, red. All hydrogen atoms are omitted for clarity.

$Ag_4L_4(P(Ph\text{-}^pCH_3)_3)_2$ units (Fig. 2g and h). The additional two L ligands capping the $Ag_4L_4(P(Ph\text{-}^pCH_3)_3)_2$ units prevent their polymerization. There are two Cl-terminated atoms at both ends of Ag_{20}, and each Cl atom caps the Ag_3 triangular face (Fig. S11, ESI†). Each silver atom of the Ag_3 triangular face is not only coordinated with Cl but also protected by S and N (deprotonation) from two quinoline ligands. The distances between Ag and Cl atoms in **Ag_{32}** were 2.589 and 2.606 Å (average 2.60 Å), which were not only much shorter than the sum of van der Waals radii of Ag and Cl atoms (1.72 Å + 1.80 Å = 3.52 Å), but also shorter than the sum of the atomic radii of Ag and Cl atoms (1.44 Å + 1.62 Å = 3.06 Å). Accordingly, the interactions between Ag and Cl atoms in **Ag_{32}** could be considered covalent interactions. The Ag–Ag bond distances of Ag_3 are 3.276 Å and 3.288 Å. The average Ag–Ag distance between the Ag atoms in the outer shell to the core in **Ag_{32}** is 2.9575 Å, which is shorter than that of **Ag_{17}** (3.3109 Å). All the thiolates in **Ag_{32}** are μ_3 coordination modes. Twelve of the -SR groups were co-coordinated with two Ag atoms in the core and one Ag atom in the shell layer, and the remaining six -SR groups were coordinated with one Ag atom in the core and two Ag atoms in the shell layer. Due to the change of the phosphine ligand (replace PPh_3 with $P(Ph\text{-}^pCH_3)_3$), the π···π interactions (Fig. S12, ESI†) and the change in steric hindrance caused by the alteration of the phosphine ligand, which affected the arrangement of the peripheral ligands, ultimately resulted in two different structures of **Ag_{17}** and **Ag_{32}**.

As illustrated in Fig. 3a and b, **Ag_{17}** and **Ag_{32}** in CH_3OH exhibit distinct UV-vis absorption spectra with molecule-like optical transitions. The UV-vis spectrum of **Ag_{17}** shows optical absorption bands at 330, 387, 487, and 597 nm. Likewise, **Ag_{32}** has absorptions at 357, 499, and 653 nm. The similar absorption in the high-energy region may derived from their similar surface structures. To gain an insight into the electronic structures and absorption characteristics of **Ag_{17}** and **Ag_{32}**, time-dependent density functional theory (TD-DFT) calculations were performed to simulate the optical absorptions (Fig. 3, Fig. S13 and S14, ESI†). The calculated UV-vis absorption spectra of **Ag_{17}** and **Ag_{32}** match well with the experimental ones with slight shifts. For **Ag_{17}**, the transition for the peaks of 423 nm is mainly from the outer shell. The lowest-energy absorption band at 618.2 nm is attributed to electronic transition from the highest occupied molecular orbital (HOMO) to the lowest unoccupied molecular orbital (LUMO). For the **Ag_{32}**, the transitions for the peaks of 362.5 nm and 451.0 nm are from the outer shell. The lowest-energy absorption band at 597.7 nm is attributed to the electronic transition from the HOMO to the LUMO. The two nanoclusters of 2e **Ag_{17}** and 8e **Ag_{32}** exhibit clear super-atomic orbital characteristics with $1S^2$ and $1S^21P^6$ (Fig. S15, ESI†).

Both **Ag_{17}** and **Ag_{32}** have emissions in the near-infrared region in solution (Fig. 4 and Fig. S16, ESI†). The **Ag_{17}** NCs in CH_3OH show the maximum emission peak remaining at 830 nm. The HOMO of **Ag_{17}** mainly lies on the Ag_5 kernel, while the LUMO is located on the surface ligands. Thus, the emission is mainly derived from the metal-to-ligand charge transfer (MLCT). The **Ag_{32}** nanocluster in CH_3OH shows the maximum emission peak at 840 nm, mainly from the mixed MLCT and cluster-centered transition. It can be found that the luminescence intensity of **Ag_{17}** is an order of magnitude higher than that of **Ag_{32}**. The quantum yield (QY) of **Ag_{17}** in the CH_3OH solution is 3.09%, while the QY of **Ag_{32}** is below 0.1%. The lifetimes of **Ag_{17}** and **Ag_{32}** are 1.47 μs and 1.61 μs (Fig. S17 and S18, ESI†), respectively, indicating phosphorescence. Similarly, the emission peak intensity of **Ag_{17}** in the near-infrared region is stronger than that of **Ag_{32}** in the solid state (Fig. S19 and S20, ESI†). As mentioned above in the structural analysis section, **Ag_{17}** has a trimeric structure of $Ag_4L_4(PPh_3)_2$ units and **Ag_{32}** has three discrete monomeric

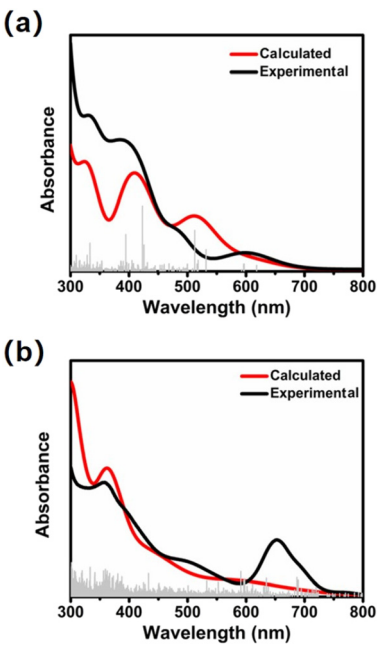

Fig. 3 Experimental (black) and calculated (red) absorption spectra of **Ag_{17}** (a) and **Ag_{32}** (b) in CH_3OH.

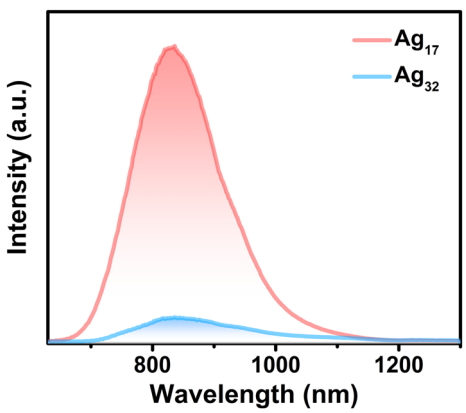

Fig. 4 Emission spectra of **Ag_{17}** and **Ag_{32}** in CH_3OH solution (excited at 400 nm).

$Ag_4L_4(P(Ph\text{-}^pCH_3)_3)_2$ units. Therefore, the rigid structure of **Ag_{17}** decreases the nonradiative decay, resulting in enhanced luminescence. Besides, rotation of the methyl groups on the phosphine ligands of **Ag_{32}** also dissipates energy, facilitating nonradiative decay that converts light into heat.[61]

Conclusions

In conclusion, we synthesized two new superatomic silver nanoclusters **Ag_{17}** and **Ag_{32}** by adjusting phosphine ligands. The structural anatomy indicated that the kernel of **Ag_{17}** is Ag_5 and the kernel of **Ag_{32}** is Ag_{20}. The inner cores of **Ag_{17}** and **Ag_{32}** have huge distinctions while the peripheral Ag–S motifs have some similarities. In addition, both the solution states and the solid states of **Ag_{17}** and **Ag_{32}** have luminescence properties in the near-infrared region. Due to the rigid structure of **Ag_{17}** and the high-frequency vibrations of the methyl groups of **Ag_{32}**, **Ag_{17}** shows stronger near-infrared emission intensity and higher QY. This work provides new insight into the construction of novel superatomic silver nanoclusters by co-reduction by regulating phosphine ligands.

Author contributions

Qing-Qing Ma and Xue-Jing Zhai: investigation, data curation, formal analysis and writing – original draft; Jia-Hong Huang: writing – original draft and validation; Yubing Si: theoretical simulation; Xi-Yan Dong: conceptualization, writing – review & editing and funding acquisition; Shuang-Quan Zang: supervision and funding acquisition; and Thomas C. W. Mak: supervision.

Conflicts of interest

There are no conflicts to declare.

Acknowledgements

This work was supported by the National Natural Science Foundation of China (No. U21A20277, 92061201), the Excellent Youth Foundation of Henan Scientific Committee (232300421022) and the Thousand Talents (Zhongyuan Scholars) Program of Henan Province (234000510007).

References

1 R. Jin, C. Zeng, M. Zhou and Y. Chen, *Chem. Rev.*, 2016, **116**, 10346–10413.
2 Z. Lei, X.-K. Wan, S.-F. Yuan, Z.-J. Guan and Q.-M. Wang, *Acc. Chem. Res.*, 2018, **51**, 2465–2474.
3 Y. Jin, C. Zhang, X.-Y. Dong, S.-Q. Zang and T. C. W. Mark, *Chem. Soc. Rev.*, 2021, **50**, 2297–2319.
4 X. Kang, Y. Li, M. Zhu and R. Jin, *Chem. Soc. Rev.*, 2020, **49**, 6443–6514.
5 Y.-M. Su, Z. Wang, C.-H. Tung, D. Sun and S. Schein, *J. Am. Chem. Soc.*, 2021, **143**, 13235–13244.
6 X.-Y. Dong, Y. Si, J.-S. Yang, C. Zhang, Z. Han, P. Luo, Z.-Y. Wang, S.-Q. Zang and T. C. W. Mak, *Nat. Commun.*, 2020, **11**, 3678.
7 M. S. Bootharaju, S. Lee, G. Deng, S. Malola, W. Baek, H. Häkkinen, N. Zheng and T. Hyeon, *Angew. Chem., Int. Ed.*, 2021, **60**, 9038–9044.
8 J.-H. Huang, Z.-Y. Wang, S.-Q. Zang and T. C. W. Mak, *ACS Cent. Sci.*, 2020, **6**, 1971–1976.
9 A. C. Templeton, W. P. Wuelfing and R. W. Murray, *Acc. Chem. Res.*, 2000, **33**, 27–36.
10 R. H. Adnan, J. M. L. Madridejos, A. S. Alotabi, G. F. Metha and G. G. Andersson, *Adv. Sci.*, 2022, **9**, 2105692.
11 F. Hu, R.-L. He, Z.-J. Guan, C.-Y. Liu and Q.-M. Wang, *Angew. Chem., Int. Ed.*, 2023, **62**, e202304134.
12 K. H. Wijesinghe, N. A. Sakthivel, T. Jones and A. Dass, *J. Phys. Chem. Lett.*, 2020, **11**, 6312–6319.
13 K. L. D. M. Weerawardene, P. Pandeya, M. Zhou, Y. Chen, R. Jin and C. M. Aikens, *J. Am. Chem. Soc.*, 2019, **141**, 18715–18726.
14 N. A. Sakthivel, M. Shabaninezhad, L. Sementa, B. Yoon, M. Stener, R. L. Whetten, G. Ramakrishna, A. Fortunelli, U. Landman and A. Dass, *J. Am. Chem. Soc.*, 2020, **142**, 15799–15814.
15 O. Lopez-Acevedo, H. Tsunoyama, T. Tsukuda, H. Häkkinen and C. M. Aikens, *J. Am. Chem. Soc.*, 2010, **132**, 8210–8218.
16 C. P. Joshi, M. S. Bootharaju, M. J. Alhilaly and O. M. Bark, *J. Am. Chem. Soc.*, 2015, **137**, 11578–11581.
17 X.-J. Zhai, J.-H. Hu, J. Guan, Y. Si, X.-Y. Dong, P. Luo, F. Pan, Z. Yu, R. Han and S.-Q. Zang, *Nano Res.*, 2023, **16**, 11366–11374.
18 S. Biswas and Y. Negishi, *J. Phys. Chem. Lett.*, 2024, **15**, 947–958.
19 R.-W. Huang, Y.-S. Wei, X.-Y. Dong, X.-H. Wu, C.-X. Du, S.-Q. Zang and T. C. W. Mark, *Nat. Chem.*, 2017, **9**, 689–697.
20 W.-M. He, Z. Zhou, Z. Han, S. Li, Z. Zhou, L.-F. Ma and S.-Q. Zang, *Angew. Chem., Int. Ed.*, 2021, **60**, 8505–8509.
21 S. Biswas, S. Das and Y. Negishi, *Nanoscale Horiz.*, 2023, **8**, 1509–1522.
22 T. Kawawaki, T. Okada, D. Hirayama and Y. Negishi, *Green Chem.*, 2024, **26**, 122–163.
23 X.-K. Wan, J.-Q. Wang, Z.-A. Nan and Q.-M. Wang, *Sci. Adv.*, 2017, **3**, e1701823.
24 Y. Lei, F. Mehmood, S. Lee, J. Greeley, B. Lee, S. Seifert, R. E. Winans, J. W. Elam, R. J. Meyer, P. C. Redfern, D. Teschner, R. Schlögl, M. J. Pellin, L. A. Curtiss and S. Vajda, *Science*, 2010, **328**, 224–228.
25 M. Cao, R. Pang, Q.-Y. Wang, Z. Han, Z.-Y. Wang, X.-Y. Dong, S.-F. Li, S.-Q. Zang and T. C. W. Mak, *J. Am. Chem. Soc.*, 2019, **141**, 14505–14509.
26 J. Yang, F. Yang, C. Zhang, X. He and R. Jin, *ACS Mater. Lett.*, 2022, **4**, 1279–1296.

27 Y. Hua, Z.-H. Shao, A. Zhai, L.-J. Zhang, Z.-Y. Wang, G. Zhao, F. Xie, J.-Q. Liu, X. Zhao, X. Chen and S.-Q. Zang, *ACS Nano*, 2023, **17**, 7837–7846.
28 Z. Yang, R. Shi, X. Liu, Q. Zhang, M. Chen, Y. Shen, A. Xie and M. Zhu, *ACS Mater. Lett.*, 2023, **5**, 2361–2368.
29 T.-H. Huang, F.-Z. Zhao, Q.-L. Hu, Q. Liu, T.-C. Wu, D. Zheng, T. Kang, L.-C. Gui and J. Chen, *Inorg. Chem.*, 2020, **59**, 16027–16034.
30 P. Luo, S. Bai, X. Wang, J. Zhao, Z.-N. Yan, Y.-F. Han, S.-Q. Zang and T. C. W. Mark, *Adv. Opt. Mater.*, 2021, **9**, 2001936.
31 M. Zhu, C. M. Aikens, F. J. Hollander, G. C. Schatz and R. Jin, *J. Am. Chem. Soc.*, 2008, **130**, 5883–5885.
32 M. W. Heaven, A. Dass, P. S. White, K. M. Holt and R. W. Murray, *J. Am. Chem. Soc.*, 2008, **130**, 3754–3755.
33 R. S. Dhayal, J.-H. Liao, Y.-C. Liu, M.-H. Chiang, S. Kahlal, J.-Y. Saillard and C. W. Liu, *Angew. Chem., Int. Ed.*, 2015, **54**, 3702–3706.
34 L. G. AbdulHalim, M. S. Bootharaju, Q. Tang, S. Del Gobbo, R. G. AbdulHalim, M. Eddaoudi, D.-E. Jiang and O. M. Bark, *J. Am. Chem. Soc.*, 2015, **137**, 11970–11975.
35 A. Desireddy, B. E. Conn, J. Guo, B. Yoon, R. N. Barnett, B. M. Monahan, K. Kirschbaum, W. P. Griffith, R. L. Whetten, U. Landman and T. P. Bigioni, *Nature*, 2013, **501**, 399–402.
36 M. Bodiuzzaman, E. Khatun, K. S. Sugi, G. Paramasivam, W. A. Dar, S. Antharjanam and T. Pradeep, *J. Phys. Chem. C*, 2020, **124**, 23426–23432.
37 L. Pen, P. Yuan, H. Su, S. Malola, S. Lin, Z. Tang, B. K. Teo, H. Häkkinen, L. Zheng and N. Zheng, *J. Am. Chem. Soc.*, 2017, **139**, 13288–13291.
38 G.-X. Duan, L. Tian, J.-B. Wen, L.-Y. Li, Y.-P. Xie and X. Lu, *Nanoscale*, 2018, **10**, 18915–18919.
39 F. Hu, J.-J. Li, Z.-J. Guan, S.-F. Yuan and Q.-M. Wang, *Angew. Chem., Int. Ed.*, 2020, **59**, 5312–5315.
40 W. Fei, S. Antonello, T. Dainese, A. Dolmella, M. Lahtinen, K. Rissanen, A. Venzo and F. Maran, *J. Am. Chem. Soc.*, 2019, **141**, 16033–16045.
41 W.-Q. Shi, Z.-J. Kuan, J.-J. Li, X.-S. Han and Q.-M. Wang, *Chem. Sci.*, 2022, **13**, 5148–5154.
42 S. Hossain, D. Suzuki, T. Iwasa, R. Kaneko, T. Suzuki, S. Miyajima, Y. Iwamatsu, S. Pollitt, T. Kawawaki, N. Barrabés, G. Rupprechter and Y. Negishi, *J. Phys. Chem. C*, 2020, **124**, 22304–22313.
43 W.-D. Tian, W.-D. Si, S. Havenridge, C. Zhang, Z. Wang, C. M. Aikens, C.-H. Tung and D. Sun, *Sci. Bull.*, 2024, **69**, 40–48.
44 C. A. Hosier and C. J. Ackerson, *J. Am. Chem. Soc.*, 2019, **141**, 309–314.
45 J. Xin, J. Xu, C. Zhu, Y. Tian, Q. Zhang, X. Kang and M. Zhu, *Chem. Sci.*, 2023, **14**, 8474–8482.
46 Y. Wang, Z. Liu, A. Mazumder, C. G. Gianopoulos, K. Kirschbaum, L. A. Peteanu and R. Jin, *J. Am. Chem. Soc.*, 2023, **145**, 26328–26338.
47 L. C. McKenzie, T. O. Zaikova and J. E. Hutchison, *J. Am. Chem. Soc.*, 2014, **136**, 13426–13435.
48 S. Biswas, S. Das and Y. Negishi, *Coord. Chem. Rev.*, 2023, **492**, 215255.
49 L. Li, Y. Zhu, B. Han, Q. Wang, L. Zheng, L. Feng, D. Sun and Z. Wang, *Chem. Commun.*, 2022, **58**, 9234–9237.
50 R. K. Gupta, L. Li, Z. Wang, B.-L. Han, L. Feng, Z.-Y. Gao, C.-H. Tung and D. Sun, *Chem. Sci.*, 2023, **14**, 1138–1144.
51 Y. Horita, S. Hossain, M. Ishimi, P. Zhao, M. Sera, T. Kawawaki, S. Takano, Y. Niihori, T. Nakamura, T. Tsukuda, M. Ehara and Y. Negishi, *J. Am. Chem. Soc.*, 2023, **145**, 23533–23540.
52 J.-J. Li, C.-Y. Liu, Z.-J. Guan, Z. Lei and Q.-M. Wang, *Angew. Chem., Int. Ed.*, 2022, **61**, e202201549.
53 E. Khatun, A. Ghosh, P. Chakraborty, P. Singh, M. Bodiuzzaman, P. Ganesan, G. Nataranjan, J. Ghosh, S. K. Pal and T. Pradeep, *Nanoscale*, 2018, **10**, 20033–20042.
54 X. Kang, S. Wang and M. Zhu, *Chem. Sci.*, 2018, **9**, 3062–3068.
55 Y. Wang, Z. Liu, A. Mazumder, C. G. Gianopoulos, K. Kirschbaum, L. A. Peteanu and R. Jin, *J. Am. Chem. Soc.*, 2023, **145**, 26328–26338.
56 Z. Liu, Y. Li, E. Kahng, S. Xue, X. Du, S. Li and R. Jin, *ACS Nano*, 2022, **16**, 18448–18458.
57 N. A. Sakthivel and A. Dass, *Acc. Chem. Res.*, 2018, **51**, 1774–1783.
58 X. Wei, Y. Lv, H. Shen, H. Li, X. Kang, H. Yu and M. Zhu, *Aggregate*, 2023, **4**, e246.
59 Z. He, Y. Yang, J. Zou, Q. You, L. Feng, M.-B. Li and Z. Wu, *Chem. – Eur. J.*, 2022, **28**, e202200212.
60 S. Nakano, T. Yoshida, H. Taniguchi and M. Yasuki, *Chem. Pharm. Bull.*, 1980, **28**, 49–56.
61 D. Xi, M. Xiao, J. Cao, L. Zhao, N. Xu, S. Long, J. Fan, K. Shao, W. Sun, X. Yan and X. Peng, *Adv. Mater.*, 2020, **32**, 1907855.